Indian Journal of Biochemistry & Biophysics
Vol. 63, March 2026, pp. 321-340
DOI: 10.56042/ijbb.v63i3.20526

Targeting neuroinflammation: Anti-alzheimer's mechanism of *Cassia fistula via in silico* approaches

Sai Kiran[1,2], Wurood A Shihab[3], Ammar A Razzak Mahmood[3], Shaik Sadik[4], Sreeharsha Nagaraja[5], Mohammed Monirul Islam[6]*, Bipindra Pandey[7], MK Mohan Maruga Raja[8] & Shankar Thapa[9]*

[1]Department of Pharmacology, KLE College of Pharmacy, Bengaluru-560 010, Karnataka, India

[2]KLE Academy of Higher Education and Research, Belagavi-590 010, Karnataka, India

[3]Department of Pharmaceutical Chemistry, College of Pharmacy, University of Baghdad, Baghdad, Iraq

[4]Department of Pharmacology; [8]Department of Pharmacognosy; & [9]Department of Pharmaceutical Chemistry, East Point College of Pharmacy, Bengaluru-560 049, Karnataka, India

[5]Department of Pharmaceutical Sciences; & [6]Department of Biomedical Sciences, College of Clinical Pharmacy, King Faisal University, Al-Ahsa 31982, Saudi Arabia

[7]Department of Pharmacy, Madan Bhandari Academy of Health Sciences, Hetauda, Nepal

Received 10 June 2025; *revised 09 August 2025*

Alzheimer's disease (AD) is a primary factor in neurodegeneration and dementia, with more research linking it to chronic neuroinflammation caused by the excessive activation of intracellular signaling pathways. This study investigates the anti-inflammatory properties of *Cassia fistula* phytoconstituents on two significant neuroinflammatory targets, SRC kinase and STAT3, using in-silico methodologies. Eleven chemicals identified by LC-MS profiling of methanolic extracts were analyzed using molecular docking utilizing AutoDock Vina v1.2.0. Fucosterol has the highest binding affinity for SRC (-10.3 kcal/mol) and STAT3 (-6.6 kcal/mol). We used Schrödinger's Desmond module to conduct a 100 ns molecular dynamics simulation to assess the stability and interactions of the fucosterol-SRC complex with other molecules. The molecule demonstrated stability in the simulation, exhibiting consistent hydrogen bonding and hydrophobic interactions. Molecular Mechanics/Generalized Born Surface Area (MM/GBSA) free energy simulations indicated favorable binding energetics. A DFT analysis demonstrated the electrical characteristics of fucosterol, highlighting a minimal HOMO-LUMO energy gap and an electrophilic potential. Principal Component Analysis (PCA) of the molecular dynamic's trajectory demonstrated minimal conformational variations, suggesting structural stability of the bound complex. This comprehensive computational investigation reveals fucosterol derived from *Cassia fistula* as a prospective natural inhibitor of neuroinflammatory signaling in Alzheimer's disease.

Keywords: Fucosterol, Natural products, Network pharmacology, Neurodegenerative disease

Alzheimer's disease (AD) is a progressive neurodegenerative disorder characterized by cognitive decline, memory impairment, and functional degradation of the brain[1]. Alzheimer's disease is the most common form of dementia, affecting more than 57 million people around the world. Because people are living longer, this number is expected to rise significantly. The illness primarily affects adults aged 60 and above, with a greater incidence noted in women. Aging, genetic predispositions, cardiovascular problems, and impaired cognitive reserve are all risk factors. The disease is becoming a bigger problem for public health around the world, especially in low- and middle-income nations where there aren't enough resources for diagnosis and care[2,3].

Pathogenic aspects of AD include amyloid-beta (Aβ) plaques, neurofibrillary tangles, and synaptic dysfunction, which can lead to neuronal death [4]. Aβ peptides, particularly the aggregation-prone Aβ42 variant, are produced by β- and γ-secretases cleaving amyloid precursor protein (APP)[5,6]. While Aβ plaques and hyperphosphorylated tau tangles have been the focus of Alzheimer's disease research, current evidence emphasizes the crucial role of neuroinflammation in its genesis and progression[7–9]. Chronic stimulation of microglia and astrocytes releases pro-inflammatory cytokines, chemokines, and ROS, producing synaptic dysfunction and neuronal death[10,11]. Src family kinases (SRC) and Signal Transducer and Activator of Transcription

*Correspondence:
E-mail: tshankar551@gmail.com, mislam@kfu.edu.sa
Suppl. data available on respective page of NOPR

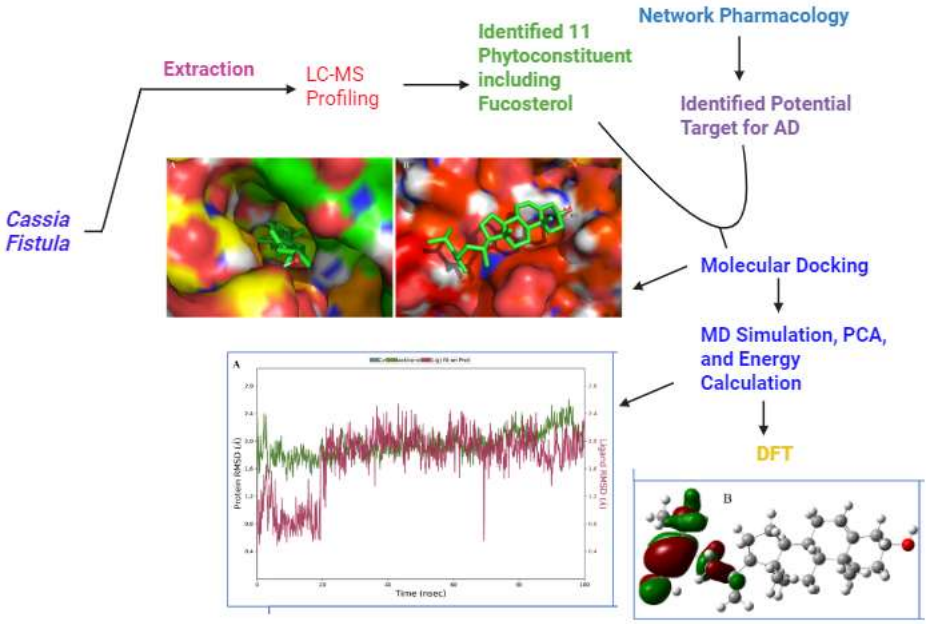

Graphical abstract

3 (STAT3) are important mediators of neuroinflammatory signaling. In Alzheimer's disease models, STAT3, a transcription factor triggered by cytokine receptors, is known to promote gliosis, induce the release of inflammatory cytokines, and alter the blood-brain barrier[12]. Non-receptor tyrosine kinases, like SRC kinases, help manage the stimulation of microglia, the flexibility of synapses, and the phosphorylation of tau [13]. The abnormal stimulation of STAT3 and SRC in Alzheimer's development suggests that blocking their specific expression may reduce the expression of inflammatory genes, restore brain balance, and slow the duration of the disease[14,15]. These kinases show promise as therapeutic targets for altering AD's neuroinflammatory processes.

Neuroinflammation is a vital component of Alzheimer's disease pathogenesis, and numerous plant-derived phytochemicals have been examined for their capacity to alter neuroinflammatory pathways. Various botanicals, including *Bacopa monnieri*[16], *Withania somnifera*[17], *Ginkgo biloba*[18], *Toddalia Asiatica*[19], and *Curcuma longa*[20], exhibit potential neuroprotective effects via antioxidant activity, inhibition of pro-inflammatory cytokines, and modulation of Aβ aggregation. The results show that medicinal plants could be a safer and more effective way to treat Alzheimer's disease than manufactured medications. *Cassia fistula*, also known as the golden shower tree, has drawn attention because of its wide range of phytochemicals and its long history of use in neuroprotection, anti-inflammation, antidiabetes, antibacterial activity, and antioxidant properties [21]. Previous studies have identified flavonoids, anthraquinones, and phenolic acids in *Cassia fistula*, many of which are acknowledged for their effects on the central nervous system and their molecular interactions with neuroinflammatory targets[22,23]. However, despite its pharmacological promise, the specific molecular interactions between the components of *Cassia fistula* and key inflammatory mediators in Alzheimer's disease remain largely neglected.

This research employed an *in silico* methodology to examine the prospective anti-Alzheimer's properties of *Cassia fistula via* the concurrent suppression of STAT3 and SRC. Computational techniques, such as network pharmacology, molecular docking, and molecular dynamics (MD) simulation, offer effective and cost-efficient strategies for the preliminary evaluation of phytocompounds concerning their binding affinity, stability, and drug-likeness before in vitro validation. These approaches speed the drug development process and provide mechanistic insights at the atomic scale[24]. This research aims to analyze the binding relationships of various *Cassia fistula* components with STAT3 and SRC in order to uncover new compounds that might lower neuroinflammation and help in Alzheimer's disease therapy.

Materials and Methods

Extraction of *Cassia fistula* Constituents

Fresh *Cassia fistula* pods were gathered, thoroughly cleaned under running tap water to remove surface dirt, and then dried in the shade for 10 to 14 days for preserving the thermolabile components. After drying, the pods were crushed and ground into a rough powder using a mechanical grinder. We measured about 200 g of the powdered substance and used a Soxhlet equipment to extract it with different solvents one after the other. To get a complete phytochemical recovery, the extraction used 70% ethanol. The extraction process lasted for eight hours, during which time the solvent in the siphon tube became clear, indicating that the extraction was complete. After the process was finished, the solvent was evaporated using a rotary evaporator at temperatures below 40°C and low pressure to make concentrated crude extracts. The extract was weighed and put in sealed containers at 4°C for later in-vitro testing. The methanolic extract, distinguished by a significant concentration of polar phytochemicals, was targeted for investigations into γ-secretase regulation and molecular docking[25].

Fourier transform infrared spectroscopy (FTIR)

FTIR spectroscopy was used to examine at the dried extract and find its unique functional groups. KBr was combined with the samples, and then they were pressed into pellets. The spectra was measured between 4000 and 400 cm^{-1}.

Liquid chromatography-mass spectrometry (LC-MS) profiling

We used LC-MS to look at the methanolic extract of *Cassia fistula* pods to find out what bioactive compounds it contained. Prior to injection, the crude extract underwent filtration through a 0.22 µm PTFE syringe filter to eliminate any particles. The solution was subsequently diluted with HPLC-grade methanol as needed. The analysis employed a high-resolution mass spectrometer alongside a UPLC Acquity H class series instrument. The separation was performed at 30°C utilizing a reverse-phase C18 column (150 mm × 2.1 mm, 1.7 µm particle size). The mobile phase consisted of solvent A, which was 0.1% formic acid in water, and solvent B, which was acetonitrile containing 0.1% formic acid. The flow rate was set at 1.2 mL/min, employing a gradient elution procedure that shifted from 5% to 95% over a duration of 10 min. It was decided that the injection volume would be 5 µL.

The mass spectrometry data were collected in both positive and negative electrospray ionization modes, covering a mass range of *m/z* 100–1000. The default settings were used to get the best source parameters. We used a Triple Quadrupole system to analyze the whole MS scans with data-dependent MS/MS fragmentation to figure out the structure. MassLynx V4.1 SCN805 software was used to process the chromatograms and mass spectra. The process of tentatively identifying phytochemicals involved the comparison of mass and MS/MS fragmentation patterns with reference databases, such as METLIN, MassBank, and the Human Metabolome Database (HMDB). Peaks linked to flavonoids, anthraquinones, phenolic acids, and other important secondary metabolites were found and sorted so that bioactivity could be linked to them later[26].

Network pharmacology

Collection and selection of phytochemical constituents

LC-MS analysis found bioactive compounds in *Cassia fistula* extract, and the PubChem database (https://pubchem.ncbi.nlm.nih.gov/ accessed on 12 February 2025) was used to check their structures. We took the SMILES codes of these compounds and put them together so that we could use them to explore targets on a computer .

Computational prediction of molecular targets

Two separate web-based technologies, Swiss Target Prediction and Super-PRED (https://prediction.charite.de/subpages/target_prediction.php), were used to find possible human protein targets for each chemical. accessed on February 15, 2025. Only targets with high confidence metrics, which are probability ratings of 0.50 or higher, were retained. To make sure the results were biologically relevant, duplicate or non-human proteins were systematically removed out.

Compilation of Alzheimer's disease-associated genes

Genes associated with Alzheimer's disease were acquired from a variety of curated repositories in order to generate a disease-specific target profile. We searched the GeneCards database (https://www.genecards.org/, retrieved on February 19, 2025) for the term "Alzheimer's disease." Genes with a relevance score of 10 or above were considered important. Also, the pseudogene and genes that weren't classified were left out.

Intersection of therapeutic targets

The overlap between the predicted targets of *Cassia fistula* phytocompounds and genes associated

with Alzheimer's was evaluated using InteractiVenn (https://www.interactivenn.net/ accessed on 28 February 2025). This intersection produced a subset of proteins with pharmacological and pathological significance, believed to mediate therapeutic effects[27].

Development of an interaction network

Using Cytoscape v3.10.2, a tri-layered network was built that included phytochemicals, possible targets, and disease relationships. In this model, nodes stood for genes or compounds, and edges stood for functional or interactional interactions. We used topological characteristics including node degree, betweenness, and closeness to find central and strongly linked molecules and targets[28].

Exploration of Protein–protein interactions

A protein-protein interaction (PPI) network was generated by employing the STRING database and a confidence threshold of 0.7 for interactions. This network was designed to investigate the relationships between overlapping protein targets. We brought the network into Cytoscape so we could see it. The CytoHubba plugin was used to find central hub proteins, and the Maximal Clique Centrality (MCC) ranking algorithm was used [29].

Functional annotation and pathway mapping

Gene Ontology (GO) analysis and Kyoto Encyclopedia of Genes and Genomes (KEGG) pathway enrichment were performed using ShinyGO 0.82 (https://bioinformatics.sdstate.edu/go/ accessed on 6 March 2025) to clarify the biological context of identified targets. Terms with p-values below 0.05 were deemed significant. The enriched biological functions and signaling pathways were presented to emphasize the key molecular mechanisms involved[30].

Molecular docking

The molecular docking study was conducted to evaluate the binding affinity and interaction profiles of phytoconstituents from *Cassia fistula* with two key neuroinflammatory targets (network pharmacology): SRC kinase and STAT3. The crystal structures of human SRC (PDB ID: 2H8H, resolution: 1.20 Å)[31] and human STAT3 (PDB ID: 6NJS, resolution: 2.70 Å)[32] were retrieved from the RCSB Protein Data Bank in .pdb format. These proteins were selected based on their known involvement in neuroinflammatory signaling and validated structural integrity.

Ligand selection and preparation

A total of 11 phytoconstituents were selected based on the results of LC-MS profiling of the methanolic extract of *Cassia fistula*. These compounds included flavonoids, anthraquinones, and phenolic derivatives previously reported for anti-inflammatory or neuroprotective activity[33]. The 2D structures of the selected ligands were obtained from the PubChem database in .sdf format and converted to 3D using Open Babel. Ligands were then energy-minimized using the MMFF94 force field and saved in pdbqt format using AutoDock Tools v1.5.7. Torsional bonds were defined to allow flexible docking[34].

Protein preparation and validation

The protein structures were cleaned by removing all crystallographic water molecules, ligands, and ions. Missing hydrogens were added, and Kollman charges were assigned using AutoDock Tools v1.5.7[35]. The prepared structures were saved in pdbqt format. The integrity and quality of the protein models were validated using Ramachandran plot analysis *via* Discovery Studio Visualizer 2021 (Fig. 1a & b) and Verify3D (https://saves.mbi.ucla.edu/ accessed on 11 March 2025) to confirm proper stereochemical quality and compatibility of 3D coordinates with amino acid sequences[36].

Docking protocol

Molecular docking was performed using AutoDock Vina v1.2.0, which supports flexible ligand–rigid receptor docking and utilizes a scoring function based on empirical free energy estimation[37]. For each protein target, a grid box (Fig. 2c and d) was defined to encompass the active site based on literature-reported binding residues:

STAT3 (6NJS): Grid center at X = 11.436, Y = 52.240, Z = 1.795 with dimensions 22 × 22 × 22 $Å^3$.

SRC (2H8H): Grid center at X = 20.485, Y = 23.415, Z = 57.633 with dimensions 20 × 20 × 20 $Å^3$.

Exhaustiveness was set to 8 to balance speed and accuracy. Each ligand was docked individually against both targets, and the top-ranked poses were selected based on binding affinity (kcal/mol) and interaction with key residues. Docking poses were visualized and analyzed using PyMOL and Discovery Studio Visualizer 2021 to identify hydrogen bonds, hydrophobic interactions, π-π stacking, and salt bridges[38].

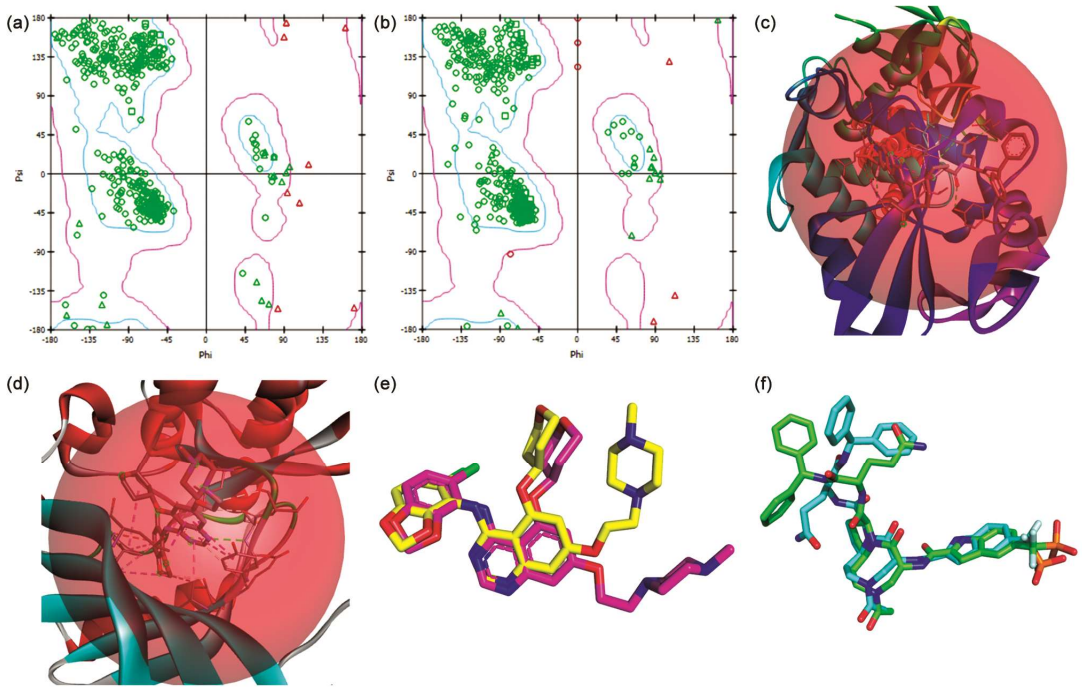

Fig. 1 — Ramchandran plot of (a) 2H8H; (b) and 6NJS. A binding cavity was generated around the co-crystal ligand of protein; (c) 2H8H; (d) 6NJS. RMSD superimpose 3D structure from redocking analysis of; and (e) 2H8H (Ser342, Gly344, Leu273, Met342, Tyr340, Leu393, Gln339, Ala293, Thr338, Ala403, Lys295, and Val281); (f)and 6NJS (Ser611, 613, 636, Arg609, Glu612, 638, Val637, Pro639, Gln644, Tyr657)

Docking process validation

The docking protocol was validated by redocking the native ligand against the binding pocket and calculating the root mean square deviation (RMSD). The ligand surface was overlapping (Fig. 2e and f), and the reported RMSD was less than 2Å, which suggests the process is accurate.

Absorption, distribution, metabolism, excretion, and toxicity (ADMET) properties prediction

ADMET properties of the selected compounds were predicted using the ADMETLab 3.0 online server (https://admetlab3.scbdd.com/ accessed on 7 August 2025). The chemical structures were provided by either uploading the SDF/MOL files, pasting the SMILES notation, or drawing them using the integrated molecular editor. After submission, the server computed key pharmacokinetic and toxicity parameters, including absorption (human intestinal absorption, Caco-2 permeability), distribution (blood–brain barrier permeability, P-glycoprotein interactions), metabolism (CYP450 inhibition/ substrate potential), excretion, and toxicity risks (hepatotoxicity, AMES mutagenicity, LD_{50}). The results were compiled into downloadable reports for further analysis, aiding in the preliminary evaluation of drug-likeness and safety profiles of the test molecules[39].

Molecular dynamics (MD) simulation

The fucosterol-SRC kinase complex was chosen due to its robust binding affinity and the positive interactions noted during molecular docking. Molecular dynamics (MD) simulation was employed to assess its dynamic stability and binding persistence. The simulation utilized the Desmond module from the Schrödinger Suite 2022-3. The receptor for the complex was the crystal structure of SRC kinase (PDB ID: 2H8H), while the ligand was the docked conformation of fucosterol, a phytosterol derived from *Cassia fistula*.

The protein-ligand complex was created via the Desmond System Builder, which included solvation in an orthorhombic simulation box with a 10 Å buffer in all directions, using the TIP3P water model. The system was neutralized with the addition of counter-ions (Na^+ or Cl^-), and the ionic concentration was adjusted to 0.15 M NaCl to simulate physiological conditions. Force field parameters were assigned *via* the OPLS4 force field to ensure precise simulation of molecular interactions. The solvated complex underwent energy reduction to resolve steric conflicts

and optimize the system's conformation. A two-stage equilibration procedure was conducted, including a 100 ps simulation in the NVT ensemble with solute constraints, followed by a 100 ps simulation in the NPT ensemble, during which the restraints were progressively relaxed. The temperature was maintained at 300 K, and the pressure was regulated at 1.01325 bar. A 100 ns molecular dynamics simulation was performed inside the NPT ensemble, with a 2-femtosecond integration time step, and trajectory data was recorded every 100 ps[40].

Post-MD simulation analysis

The post-simulation study used the Simulation Interaction Diagram tool inside Maestro. The root mean square deviation (RMSD) of the protein backbone and ligand was computed to evaluate overall structural stability. The root mean square fluctuation (RMSF) of protein residues was examined to assess local flexibility. The radius of gyration (Rg) was assessed to determine the compactness of the protein structure over time. The quantity and stability of hydrogen bonds and hydrophobic interactions between fucosterol and SRC kinase were analyzed throughout the trajectory[41].

Principal component analysis (PCA)

The trajectory file (.dtr) of the fucosterol-SRC complex was used as input for PCA analysis after the 100-nanosecond MD simulation in Desmond was finished. The Simulation Event Analysis tool in Maestro was used to do PCA. In order to eliminate translational and rotational motions, the trajectory was first aligned to the reference frame using the protein's Cα atoms. Covariance analysis was conducted on the positional variations of the Cα atoms to identify the principal components (PCs). To identify the main motions that contribute to conformational variability, the first three principal components (PC1, PC2, and PC3) were shown. The interpretations sought to assess collective motions that impact ligand binding and protein function, such as loop shifts and domain flexibility[42].

Molecular mechanics/generalized born surface area (MM/GBSA) energy calculations

The Thermodynamic Integration module in Schrödinger's Prime interface was used to estimate the binding free energy on representative frames of the equilibrated trajectory. In order to reach equilibrium, the trajectory was restricted to the last 20 ns. Frames were extracted at intervals of 10 ns, for a total of 10 frames. Every frame underwent MM/GBSA analysis using the OPLS4 force field and the VSGB 2.1 implicit solvation model. Equation 1 was used to calculate the total binding free energy (ΔG_bind).

$$\Delta Gbind = Gcomplex - (Gprotein + Gligand) \quad \ldots(1)$$

Where:

The terms Gcomplex, Gprotein, and Gligand refer to the lowered free energies of the unbound ligand, protein-ligand complex, and unbound protein, respectively. To make it easier to grasp the fundamental driving elements behind binding, the contributions from van der Waals interactions, electrostatics, solvation energy, and surface area were also given separately[43].

Density functional theory (DFT)

Density functional theory calculations were performed with Gaussian 16 to investigate the electrical characteristics of fucosterol. The molecular geometry was optimized using the B3LYP functional with the 6-31G(d,p) basis set in the gas phase. A frequency study was conducted to ascertain the absence of imaginary frequencies, so validating that the structure constitutes a genuine energy minimum.

$$\eta \frac{ELUMO - EHOMO}{2},$$
$$\omega = \frac{\mu 2}{2\eta}, \qquad \mu = \frac{EHOMO + ELUMO}{2} \quad \ldots(2)$$

The energies of the highest occupied molecular orbital (HOMO) and the lowest unoccupied molecular orbital (LUMO) were calculated to ascertain the HOMO-LUMO energy gap (ΔE), offering insights on the molecule's chemical reactivity and stability. Global properties including chemical hardness (η), electrophilicity (ω), and chemical potential (μ) were obtained from orbital energies (Eq. 2). Molecular Electrostatic Potential (MEP) maps were produced using GaussView to illustrate potential reactive sites[44]. The quantum chemical characteristics enabled the analysis of fucosterol's interaction with SRC kinase, as demonstrated in docking and molecular dynamics simulations.

Results and Discussion

Extraction yield

The ethanolic extract of *Cassia fistula* formed 4.34%.

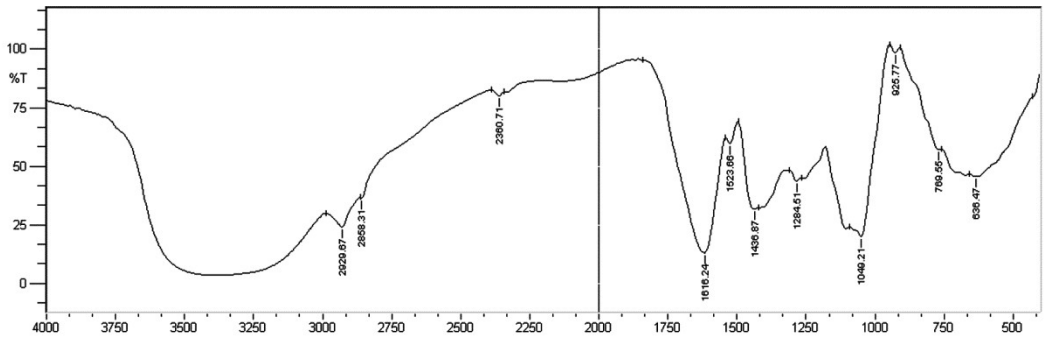

Fig. 2 — FT-IR spectrum of *Cassia fistula* extract showing characteristic absorption bands corresponding to various functional groups.

Table 1 — Predicted phytoconstituents from the ethanolic extract of *Cassia fistula* and their *m/z* value, molecular weight (MW), fragments, and classification.

S. No	Phytoconstituents	*m/z* $(M+H)^+/(M-H)^-$	MW	RT	Fragments	Classification
1.	Rhein	283	284	8.3	211, 143, 117, 57	Anthraquinone
2.	Catechin	292	290	3.1	175, 131, 113, 69	Flavanol (Polyphenol)
3.	Chrysophanic acid	253	254	NA	132, 113, 69	Anthraquinone
4.	Quercetin	301	302	4.9	205, 149	Flavonoid
5.	Ellagic acid	303	202	5.3	209, 113, 71	Polyphenol
6.	Elemicin	209	208	NA	113, 75, 71	Aromatic ether
7.	Physcion	283	284	43.0[48]	211, 143, 117, 57	Methoxylated anthraquinone
8.	Esculin	339	340	3.7	311, 175, 69	Coumarin glycoside
9.	Betaine	117	117	2.54	115	Zwitterion
10.	Fucosterol	411	412	20-22[49]	339, 133, 113, 69	Sterol
11.	Sitosterol	414	414	15-20[50]	339, 133, 113, 69	Sterol

FT-IR spectra interpretation

Functional groups related with *Cassia fistula* extract's neuroprotective bioactive compounds were identified from its FT-IR spectra. Absorption bands at 3269 cm^{-1} and 2920 cm^{-1} indicate alcohols and aliphatic hydrocarbons, respectively, due to O–H and C–H stretching vibrations. A peak at 2360 cm^{-1} may indicate –C≡C– or –C≡N– groups, but may also indicate CO_2 interference.

The absorption band at 1618 cm^{-1} suggests C=O stretching from conjugated ketones or amides. Peaks at 1429, 1384, and 1266 cm^{-1} are related with bending vibrations of aromatic amines (CH_2/CH_3 groups) and C–N stretching. A distinct band at 1040 cm^{-1} indicates C–O–C stretching, indicating ethers or esters. Aromatic rings were confirmed by bands at 929 cm^{-1}, 706 cm^{-1}, and 639 cm^{-1}, indicating out-of-plane bending vibrations (Fig. 2). The spectrum indicates that *Cassia fistula* includes phenolics, alcohols, esters, and amines, which may contribute to its anti-inflammatory and neuroprotective properties for Alzheimer's disease treatment.

LC-MS characterization of *Cassia fistula*

The LC-MS analysis of the ethanolic extract of *Cassia fistula* tentatively identified several phytoconstituents based on their *m/z* values, molecular weights (MW), retention times (RT), fragment ions, and classifications.

Several phytoconstituents were tentatively identified from the ethanolic extract of *Cassia fistula* using LC-MS analysis. Rhein (*m/z* 283, MW 284) eluted at 8.3 min, with characteristic fragments at 211, 143, 117, and 57, confirming it as an anthraquinone (Table 1). Catechin (*m/z* 292, MW 290) was detected at 3.1 min, while chrysophanic acid (*m/z* 253, MW 254) eluted after 20 min in a published report[45]; both exhibited fragment ions consistent with their known structures. Quercetin (*m/z* 301, MW 302) and ellagic acid (*m/z* 303, MW 302) were identified at 4.9 and 5.3 min, respectively (Fig. 3), with fragmentation patterns typical of flavonoid and polyphenol compounds. Elemicin (*m/z* 209, MW 208) and physcion (*m/z* 283, MW 284) were detected without recorded retention times, based on their specific fragmentation profiles.

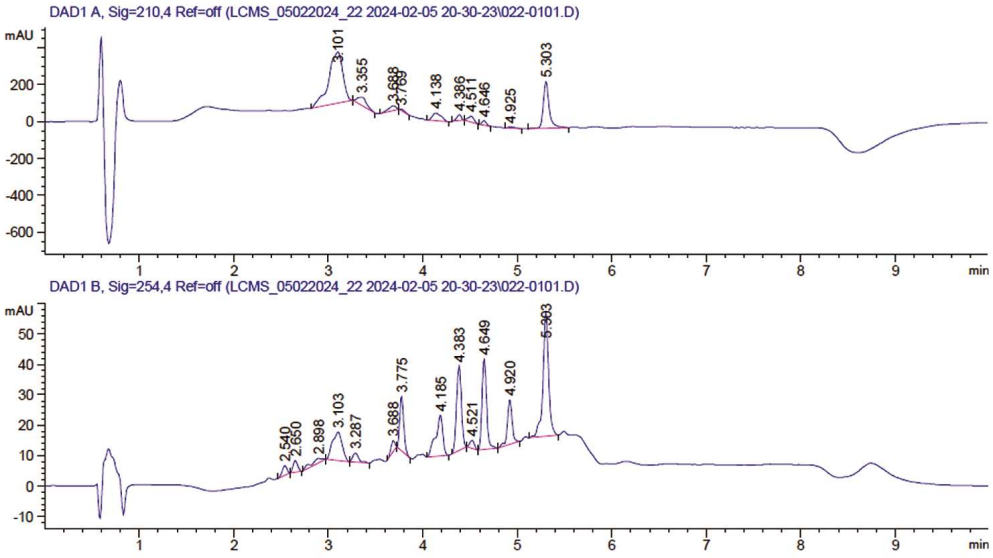

Fig. 3 — Chromatogram of ethanolic extract of *Cassia fistula*

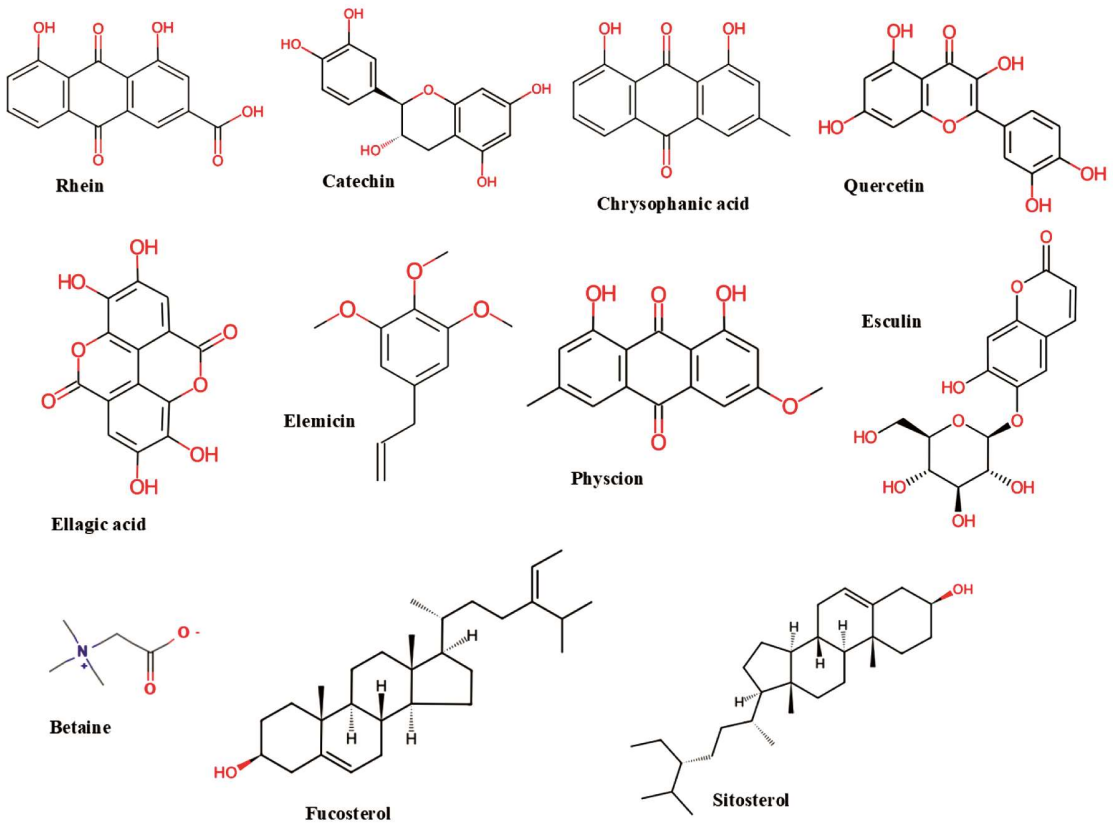

Fig. 4 — LC-MS predicted phytoconstituents from *Cassia fistula*

Esculin (*m/z* 339, MW 340) appeared at 3.7 min, showing fragments characteristic of coumarin glycosides. Betaine (*m/z* 117, MW 117) eluted early at 2.54 min, confirming its zwitterionic nature. Lastly, sterols including fucosterol (*m/z* 411, MW 412) and sitosterol (*m/z* 414, MW 414) were identified based on common fragment ions. However, sterol derivatives generally eluted around 15 to 25 min[46,47]. Figure 4 represents the 2D structure of the predicted 11 phytoconstituents.

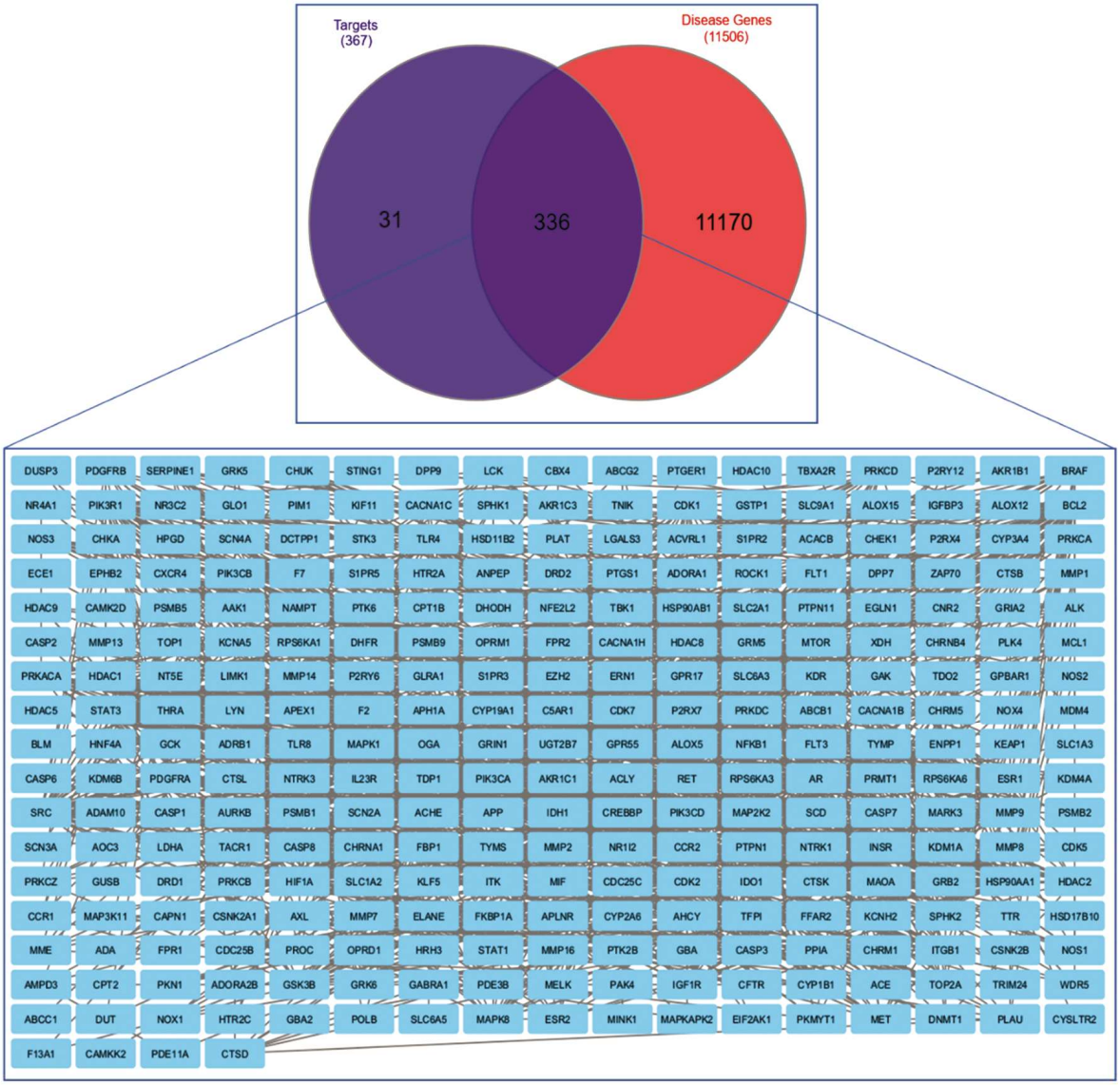

Fig. 5 — Common gene between compounds (a) (*Cassia fistula*) target; (b) and AD gene and protein-protein interaction

The mass fragmentation spectra are given in the (Suppl. Fig. S1 to S6).

Network pharmacology

Common gene and PPI network

In the network pharmacology analysis, a total of 367 potential targets of phytoconstituents from *Cassia fistula* were identified. These were compared with 11,506 Alzheimer's disease (AD)-associated genes to find common targets. As shown in Figure 5A, 336 overlapping genes were identified, indicating significant target relevance between *Cassia fistula* compounds and AD pathology. A small subset of 31 targets was unique to the compounds, while 11,170 genes were specific to AD. Further, the common targets were subjected to a protein-protein interaction (PPI) analysis (Fig. 5B). The PPI network revealed extensive interactions among the 336 overlapping genes, highlighting critical nodes potentially involved in the modulation of Alzheimer's disease processes.

Identification of key target genes through network topology analysis

Max clique centrality (MCC), degree, and proximity measures were used to rank potential targets using network topology analysis. MCC values indicated SRC, STAT3, STAT1, GRB2, PTPN11, HSP90AA1, PIK3R1, PIK3CA, ESR1, and LYN as the 10 most important genes (Fig. 6A). The genes' enhanced centrality scores indicate their importance in network stability and biological regulation. Major

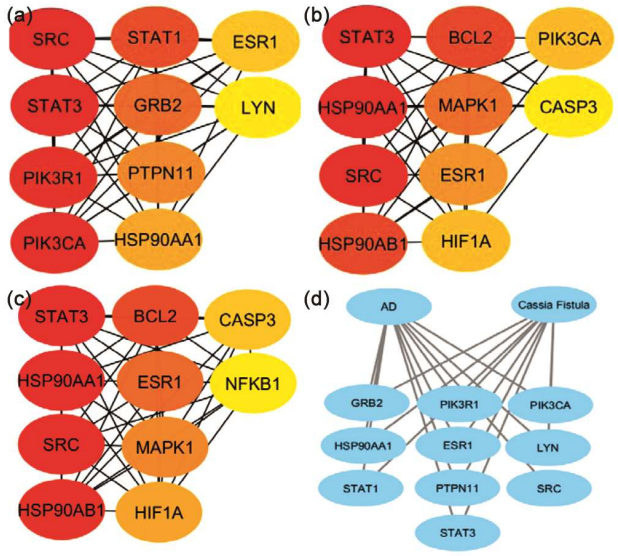

Fig. 6 — Top ten best genes based on (a) MCC, (b) Degree, and (c) Closeness, and (d) *Cassia fistula* & AD common gene interactions

hub genes are shown in (Fig. 6b and c) using degree and closeness methods. *Cassia fistula* compounds interact with Alzheimer's genes (Fig. 6d). The interaction map showed that *Cassia fistula* and Alzheimer's disease share molecular interactions with genes like SRC, STAT3, PIK3R1, PIK3CA, GRB2, HSP90AA1, STAT1, PTPN11, ESR1, and LYN, supporting the idea of a dual therapeutic mechanism that modulates these essential targets.

Enrichment analysis of common targets: Pathway, Biological Process, and Cellular Component Associations

Enrichment studies showed that *Cassia fistula* targets are linked to key networks such EGFR signaling, hormone control, and immune responses. Figure 7A shows that gene Ontology analysis showed participation in biological processes such hormone regulation and cellular response to stimuli, as well as location in critical cellular structures like the phosphatidylinositol 3-kinase complex and endoplasmic.

The positive control of lamellipodium organization, the insulin receptor signaling pathway, and various responses to stimuli like peptides, hormones, and nitrogenous compounds were found in Gene Ontology biological process enrichment (Fig. 7b). This shows that active substances affect several biological events linked to cellular communication and metabolic control.

KEGG pathway

KEGG pathway analysis of the prolactin signaling cascade identifies potential targets for Alzheimer's disease (AD), such as PI3K, c-Src, Grb2, STAT, and ERα/β (Fig. 8). Red proteins are critical locations where *Cassia fistula* compounds may be neuroprotective. PI3K and c-Src are essential to the PI3K-Akt signaling pathway, which increases neuronal survival and inhibits apoptosis in Alzheimer's disease. Activating this pathway may slow neurodegeneration. Gab2, an Alzheimer's risk factor, affects tau phosphorylation and amyloid-beta toxicity. It must be regulated to reduce disease pathogenicity. STAT, part of the Jak-STAT pathway, mediates brain inflammation. Overactivation is a key target for anti-inflammatory therapy in Alzheimer's disease because it causes chronic neuroinflammation. Estrogen receptors (ERα and ERβ) enhance neuroprotection by promoting synaptic plasticity and reducing oxidative stress. Their reduction post-menopause correlates with an elevated risk of Alzheimer's disease.

Molecular docking analysis

The molecular docking research revealed varying binding affinities of *Cassia fistula* phytoconstituents for SRC kinase (PDB ID: 2H8H) and STAT3 (PDB ID: 6NJS). Amino acid residues frequently observed in prominent binding ligands for SRC kinase comprise Met341, Thr338, and Glu339. Similarly, for STAT3, Ser613, Arg609, and Glu612 were the most frequently targeted residues. Among the tested compounds, fucosterol demonstrated the strongest binding affinity with SRC kinase, recording a binding score of -10.3 kcal/mol. This was closely followed by the co-crystal ligand (-10.2 kcal/mol) and dasatinib, the reference drug (-9.9 kcal/mol). Fucosterol interacted with Met341, a residue commonly engaged by other top-ranking ligands, through one hydrogen bond (2.5Å). On the contrary, betaine exhibited the weakest binding affinity toward both SRC kinase and STAT3, with a docking score of -3.6 kcal/mol and no detectable interactions in SRC, and a single hydrogen bond (1.95 Å) with Ser613 in STAT3 (Table 2).

Fucosterol perfectly aligns with the binding pocket of both proteins (Fig. 9a and b). In the STAT3 docking studies, fucosterol showed the most potent interaction (-6.6 kcal/mol), engaging Glu612 via one hydrogen bond (2.1Å). Interestingly, ellagic acid also exhibited a similar binding affinity (-6.5 kcal/mol). However, the co-crystal ligand again exhibited the strongest affinity (-8.9 kcal/mol), forming seven hydrogen bonds with residues including Ser613,

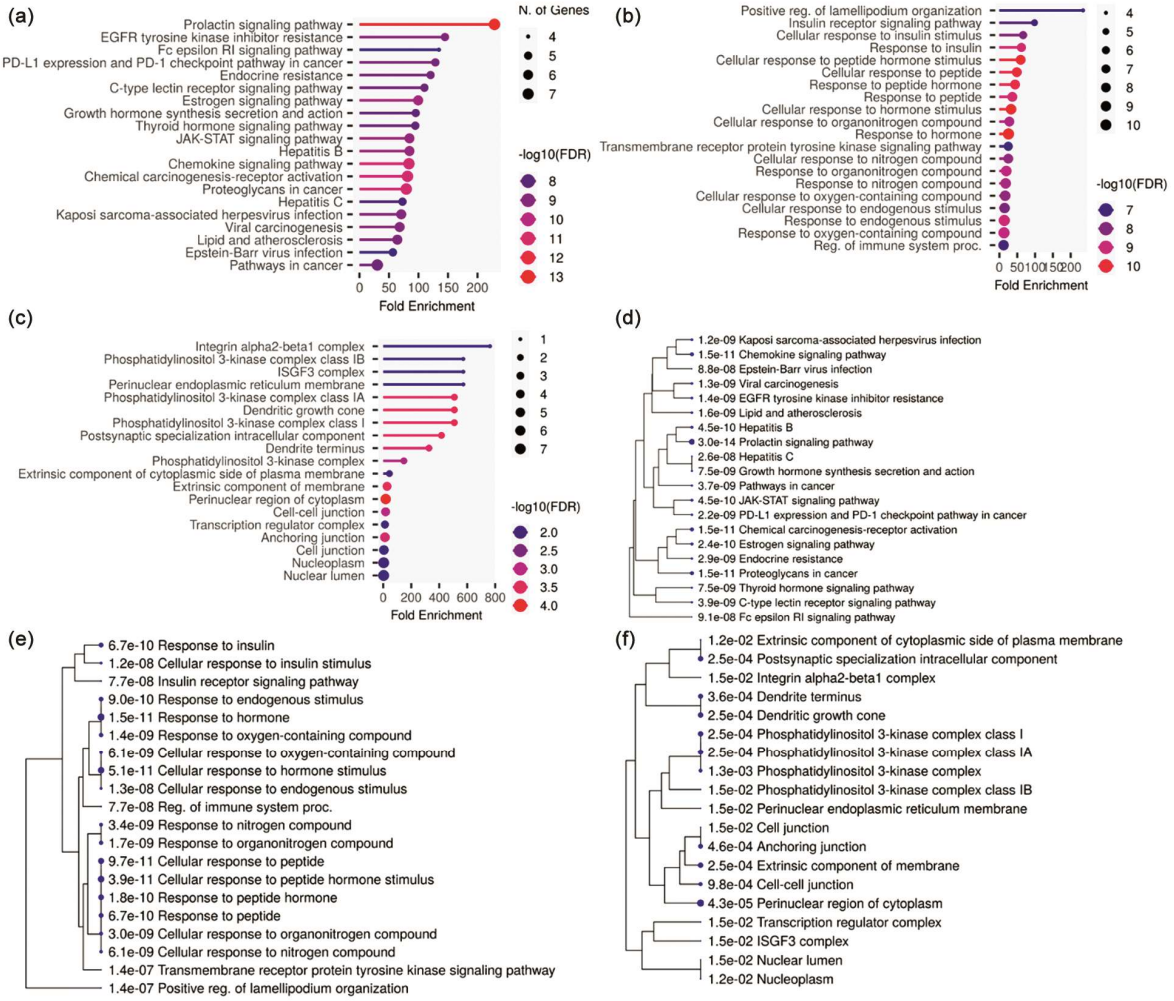

Fig. 7 — Bar plot of (a) EGFR; (b) GO biological; (c) GO chemical component; (d) tree plot of EGFR; (e) GO biological; and (f) GO chemical component

Glu612, and Arg609 residues also commonly involved with other ligands. These acids belong to the SH2 domain, which is essential for DNA binding and STAT3 dimerization. One known method of reducing STAT3 activity is disruption of SH2 sites[51]. Ellagic acid demonstrated outstanding efficacy as a phytoconstituent for STAT3, interacting with three identical residues as the co-crystal ligand: Ser611, Ser613, and Arg609. These interactions suggest it may competitively inhibit STAT3 function and interfere with its downstream signaling, which is involved in neuroinflammation and neurode generation pathways in Alzheimer's disease[52,53]. Quercetin and esculin significantly interacted with several residues shared by the co-crystal ligand and dasatinib, hence enhancing their potential as dual-target inhibitors. The repetition of Ser613 and Arg609 among high-affinity ligands reinforces the notion that these residues are crucial for efficient STAT3 suppression. The 2D molecular interactions of all phytoconstituents against both proteins are presented in the (Suppl. Figs. S7-S30). The alignment of binding affinity data and prevalent amino acid interactions among high-performing drugs highlights their promise for further advancement as multitarget therapies for Alzheimer's disease.

ADMET properties analysis

The docking results revealed that fucosterol exhibited significant binding affinity for both proteins. The ADMET characteristics of fucosterol were examined. Fucosterol's radar map of ADMET features shows its pharmacokinetic and toxicological profile in respect to the lower and upper limit ranges. Figure 10 shows that most values are within the optimal range for absorption, distribution,

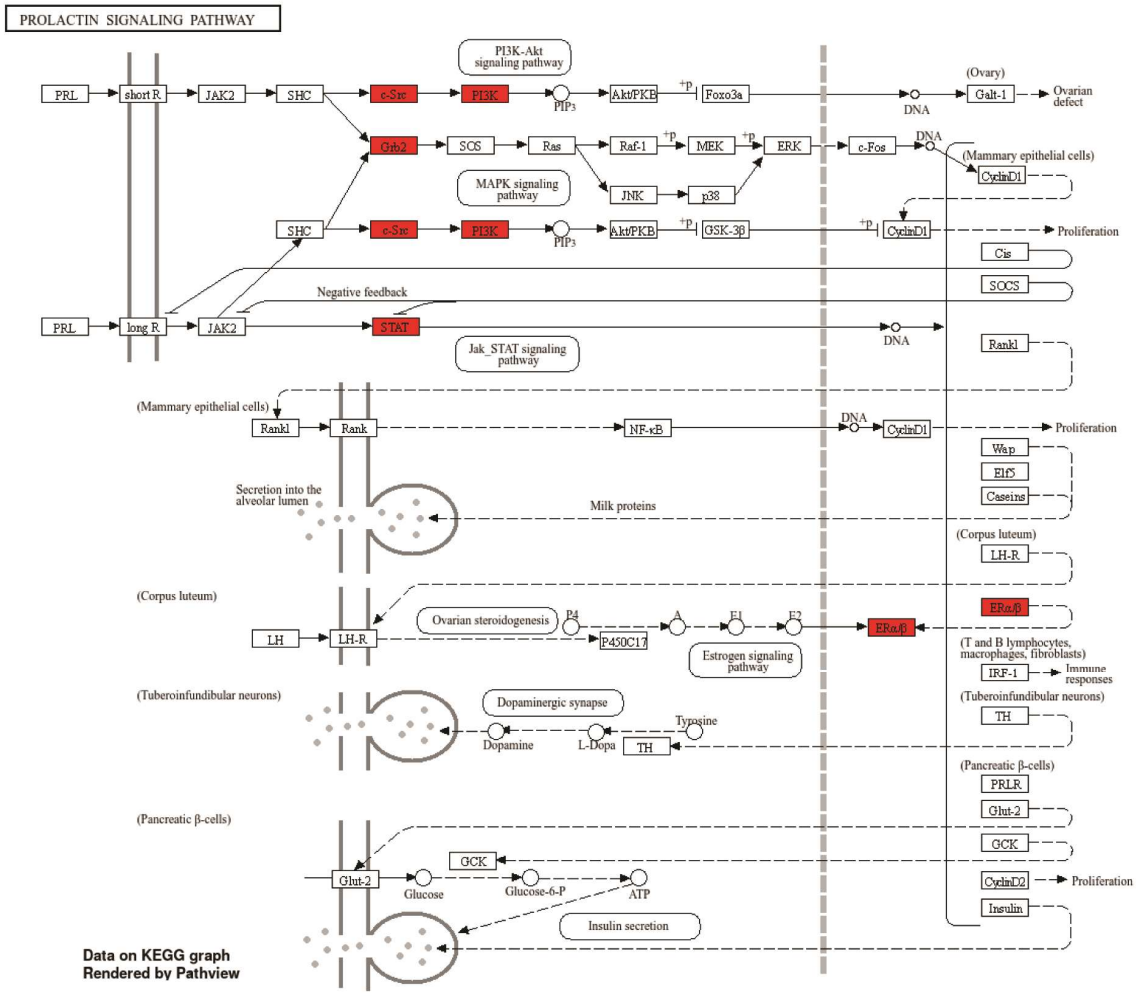

Fig. 8 — The Prolactin Signaling Pathway KEGG pathway map shows red molecular targets connected to Alzheimer's disease pathogenesis. Targets such as PI3K, c-Src, Grb2, STAT, and ERα/β are involved in neuroinflammation, neuronal survival, and estrogen-mediated neuroprotection, suggesting possible therapeutic targets for *Cassia fistula* bioactive substances

metabolism, and excretion. Fucosterol's ADMET prediction shows high lipophilicity (logP = 7.69), suggesting hydrophobicity that may affect solubility and permeability. Poor Caco-2 permeability (–5.14) and low chances of P-gp inhibition (0.0337) and substrate potential (0.0085) imply little P-glycoprotein interaction. Fucosterol shows a high probability for BCRP interaction (0.8205) but low for BSEP inhibition (0.0419) and BBB penetration (0.0027) (Table 3). CYP enzyme inhibition/ substrate potential is negligible, indicating low metabolic interference risk. Toxicity predictions suggest moderate carcinogenicity (0.7824) and nephrotoxicity (0.5698), while probabilities for AMES mutagenicity, DILI, genotoxicity, neurotoxicity, and ototoxicity remain low, supporting a generally acceptable safety profile.

MD simulation

From the docking results, fucosterol showed promising activity as SRC kinase inhibition. Therefore, we have taken the fucosterol-SRC kinase complex for MD simulation. To further validate the docking results, MD simulation of the fucostero l–SRC kinase complex was performed for 100 ns. The RMSD analysis (Fig. 11a) revealed that the SRC kinase backbone remained structurally stable, with fluctuations ranging between 1.2 Å and 2.2 Å. After 20 ns, the ligand RMSD stabilized and maintained a range of 1.5-2.0 Å throughout the simulation. This stability means fucosterol maintained a consistent active site binding configuration throughout the simulation. The RMSF of protein residues (Fig. 11b) confirmed the core structure's stiffness, with only a few flexible loop sections showing substantial fluctuations (up to 4.5 Å), particularly around

Table 2 — Molecular docking results of *Cassia fistula* phytoconstituents against SRC kinase (PDB ID: 2H8H) and STAT3 protein (PDB ID: 6NJS).

S. No	Phytoconstituents	Binding Score (kcal/mol)	Binding Amino Acids	No of H-bonds	H-Bond Distance (Å)
			SRC Kinase (2H8H)		
1.	Rhein	-9.5	Met341	1	2.46
2.	Catechin	-8.9	Met341, Asp404	2	2.07, 2.10
3.	Chrysophanic acid	-9.4	Met341, Glu339, Thr338	5	(1.81, 2.30, 2.47), 2.85, 2.08
4.	Quercetin	-9.0	Met341, Glu339, Thr338, Leu273	4	1.80, 2.49, 2.64, 2.57
5.	Ellagic acid	-9.1	Met341, Thr338, Asp303	3	2.62, 1.97, 2.63
6.	Elemicin	-6.1	Lys295, Thr338	2	3.32, 2.50
7.	Physcion	-9.4	Met341	1	2.45
8.	Esculin	-8.7	Phe405	1	2.76
9.	Betaine	-3.6	-	-	-
10.	Fucosterol	-10.3	Met341	1	2.5
11.	Sitosterol	-9.7	Asp348	1	1.74
12.	Dasatinib (Reference drug)	-9.9	Thr338, Arg388	2	2.98, 2.12
13.	Co-crystal ligand	-10.2	Met341	1	2.10
			STAT3 (6NJS)		
1.	Rhein	-6.3	-	-	-
2.	Catechin	-6.2	Gln644	1	2.85
3.	Chrysophanic acid	-5.9	Lys658	1	2.30
4.	Quercetin	-6.2	Glu638, Gln644	2	2.21, 2.08
5.	Ellagic acid	-6.5	Ser611, Ser613, Arg609	3	2.69, 2.47, 2.37
6.	Elemicin	-4.5	Arg609	1	2.01
7.	Physcion	-6.0	Ser613, Arg609	4	2.46, (1.92, 5.90, 3.10)
8.	Esculin	-6.1	Ser613, Glu612, Ser611, Arg609	5	1.98, 2.52, 2.30, (2.13, 2.11)
9.	Betaine	-3.6	Ser613	1	1.95
10.	Fucosterol	-6.6	Glu612	1	2.1
11.	Sitosterol	-5.8	-	-	-
12.	Dasatinib (Reference drug)	-7.1	Glu638, Arg609, Ser636, Ser613, Ser614	5	2.94, 2.36, 3.04, 2.52, 2.67
13.	Co-crystal ligand	-8.9	Ser613, Glu612, Arg609, Tyr657, Ser636	7	1.77, (2.30,2.40), 5.46, (2.77, 2.70), 3.04

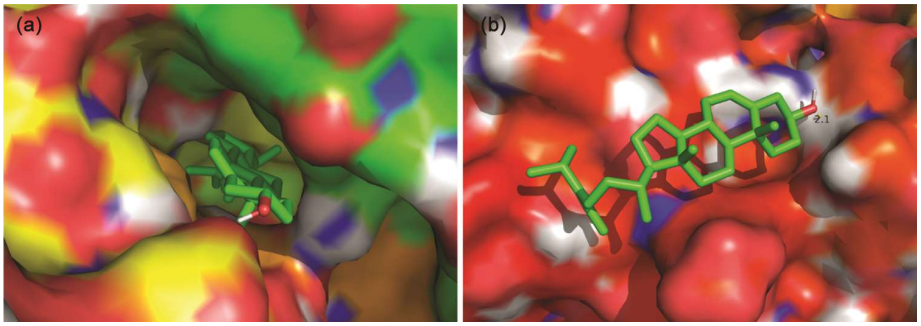

Fig. 9 — Molecular docking interaction of fucosterol against A) SRC (2H8H) and B) STST3 (6NJS) proteins visualized in surface model.

residue indices 50-150 and 200-250. The RMSF analysis of fucosterol atoms (Fig. 11c) showed little internal flexibility, with most atoms showing variations below 1.5 Å, indicating stable ligand conformational dynamics in the binding pocket. Fucosterol's robust and long-lasting association with SRC kinase suggests it may be an effective Alzheimer's disease kinase inhibitor.

The fucosterol-SRC kinase complex's structural and interactional stability was examined using

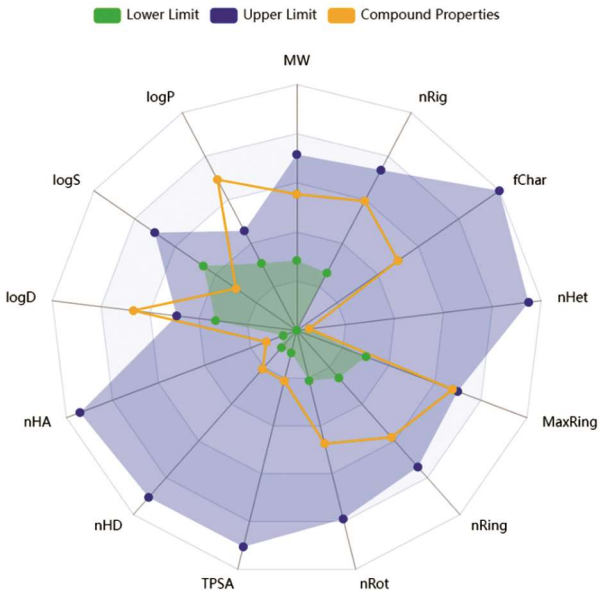

Fig. 10 — Fucosterol Radar view of ADMET properties

Table 3 — ADMET properties of fucosterol

Parameters	Value/Probability
logP	7.6958353
caco2	-5.135924
pgp_inh	0.0336777
pgp_sub	0.0084635
BCRP	0.8205383
BSEP	0.0419755
BBB	0.0026895
CYP1A2-inh	2.18E-05
CYP1A2-sub	3.64E-10
CYP2C19-inh	5.31E-05
Ames	0.085726
Carcinogenicity	0.7823956
DILI	0.1658922
Genotoxicity	0.0186606
Nephrotoxicity-DI	0.5698307
Neurotoxicity-DI	0.0680921
Ototoxicity	0.4419477

trajectory-based metrics (Fig. 12a). In the 100 ns simulation, the Rg remained stable at an average of 5.0 Å, showing that the protein remained in its tight shape without unraveling The complex's molecular surface area (MolSA) remained stable at 422-426 Å², indicating constant surface exposure (Fig. 12a). After 20 ns, the solvent-accessible surface area (SASA) decreased and stabilized, indicating structural changes or ligand-induced stability buried hydrophobic regions. Polar surface area (PSA) results consistently varied from 48 to 50 Å², confirming persistent polar interactions across time.

Met341 was the most consistently interacting residue, sustaining persistent connections with fucosterol for 80% of the simulation time, showing its role in ligand stability (Fig. 12b and 13a). A constant Met341 interaction over the 100 ns protein-ligand contact period (Fig. 13b) corroborated these results. Additional residues, including Leu273, Ala293, Phe307, Met314, Leu317, Val323, Leu325, Tyr340, Ser342, and Gly344, contributed to ligand stabilization through hydrophobic contacts and transient interactions (Fig. 14b). Gly344 and Ser342 were stable, although Leu407 and Phe405 showed minimal but notable interactions from early to mid-simulation. Fig. 13B's top panel revealed stable ligand anchoring in the binding pocket with consistent interactions each frame. Met341, a binding anchor, kept Fucosterol's interaction network stable.

Post-MD simulation analysis

SRC kinase–fucosterol complex conformational dynamics and stability were revealed by post-MD modeling (Fig. 14). Numerous low-energy basins indicate energetically favorable structure states in a 2D Free Energy Landscape (FEL) picture. Basin distribution in unique PC1-PC2 space shows high system conformational flexibility. A global energy minimum and many shallow local minima were seen in the 3D FEL plot, indicating dynamic metastable state shifts throughout the simulation track.

Color-coded 3D PCA projections illustrated the system's temporal development inside the principle component space (PC1, PC2, PC3). The system may be nearing equilibrium owing to a directed conformational change rather than random fluctuations. PC1 and PC2 had bimodal probability density functions (PDFs), notably PC2, suggesting that the system occupied two key conformational states throughout simulation (Fig. 15). The fucosterol-SRC kinase complex demonstrated structural heterogeneity, preferring stable and energetically beneficial conformations, validating its dynamic but stable binding behavior in simulation.

MM/GBSA calculation

The MM-GBSA investigation showed persistent and beneficial ligand-target protein binding. The binding free energy (ΔG_bind) had a steady average of -74.93 kcal/mol over the 100 ns simulation, demonstrating a robust and lasting connection

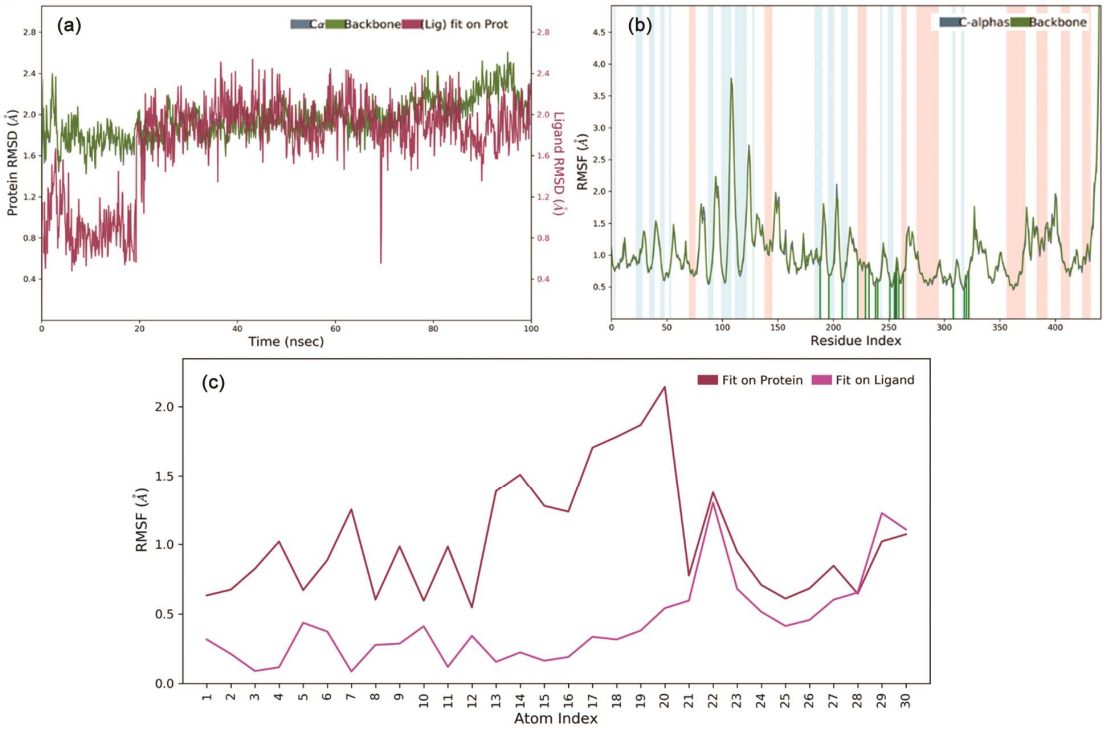

Fig. 11 — (a) RMSD plot of fucosterol-SRC kinase complex; (b) RMSF plot of SRC kinase; and (c) fucosterol

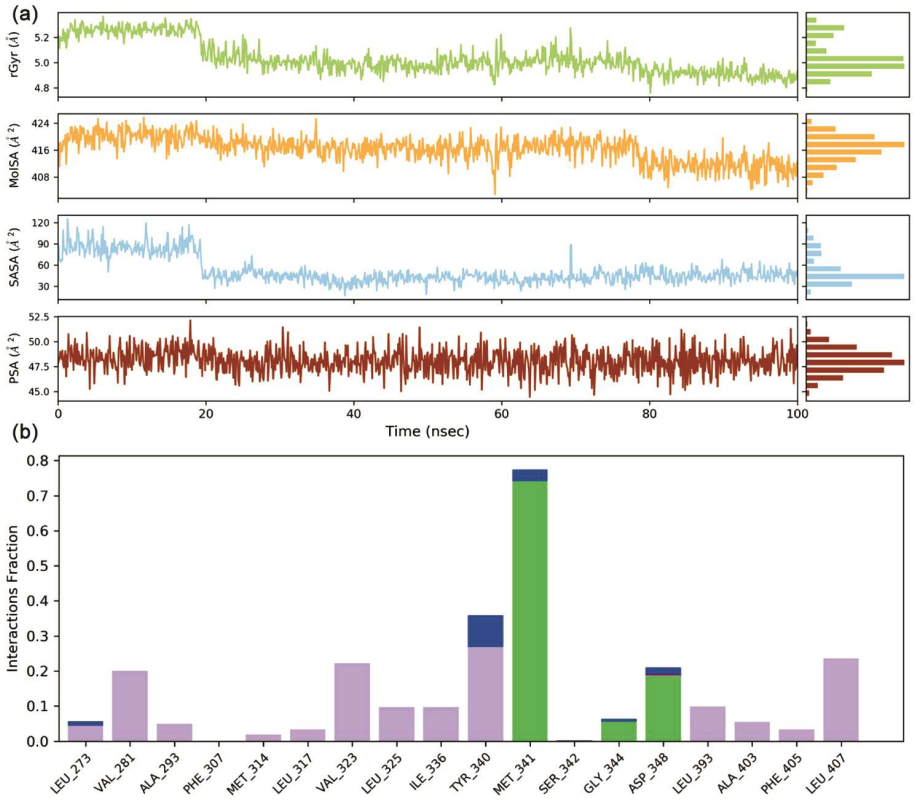

Fig. 12 — (a) Molecular Surface Area (MolSA), Solvent Accessible Surface Area (SASA), and (b) Polar Surface Area (PSA) of the protein-ligand combination and SRC kinase-fucosterol interaction. The interaction profile showed hydrophobic contacts (purple), hydrogen bonds (blue), and water bridges (green), suggesting multimodal binding

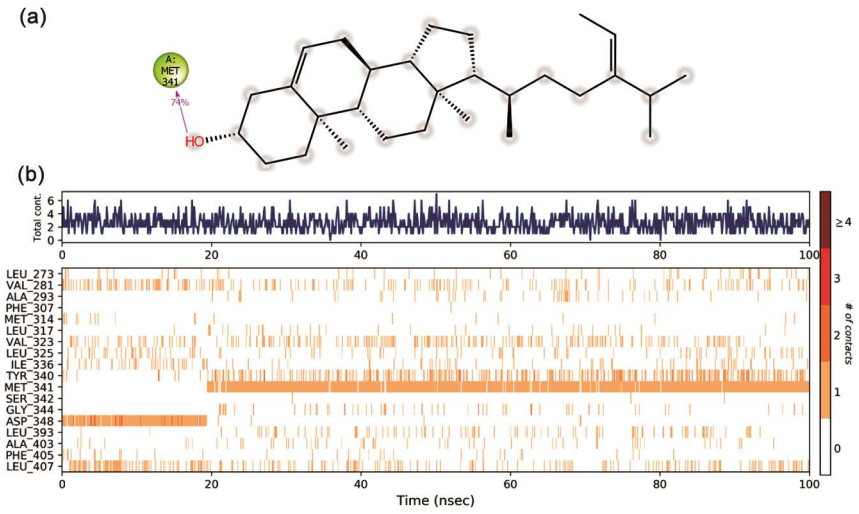

Fig. 13 — 2D molecular interaction of fucosterol against (a) protein; and (b) protein-ligand contact timeline

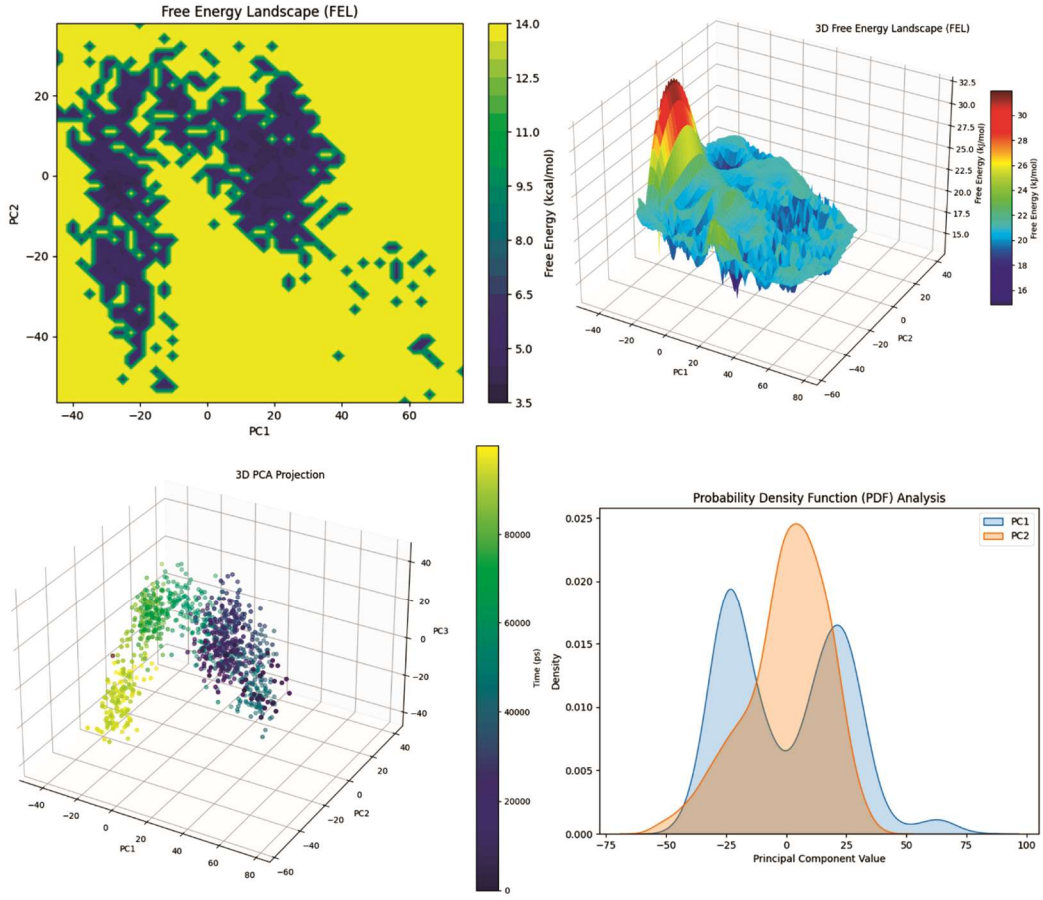

Fig. 14 — Analysis of the free energy landscape (FEL), three-dimensional FEL, three-dimensional PCA projection, and probability density function (PDF) for the SRC kinase-fucosterol complex

(Fig. 15a). The distribution of energy components in (Fig. 15b) shows that van der Waals (-49.91), Coulombic (-19.86), and lipophilic (-29.75) interactions significantly affect binding affinity. Hydrogen bonding (-1.98) and covalent interactions (-4.91) have no effect. Figure 15c showed appropriately distributed energy component histograms centered at their means, validating these

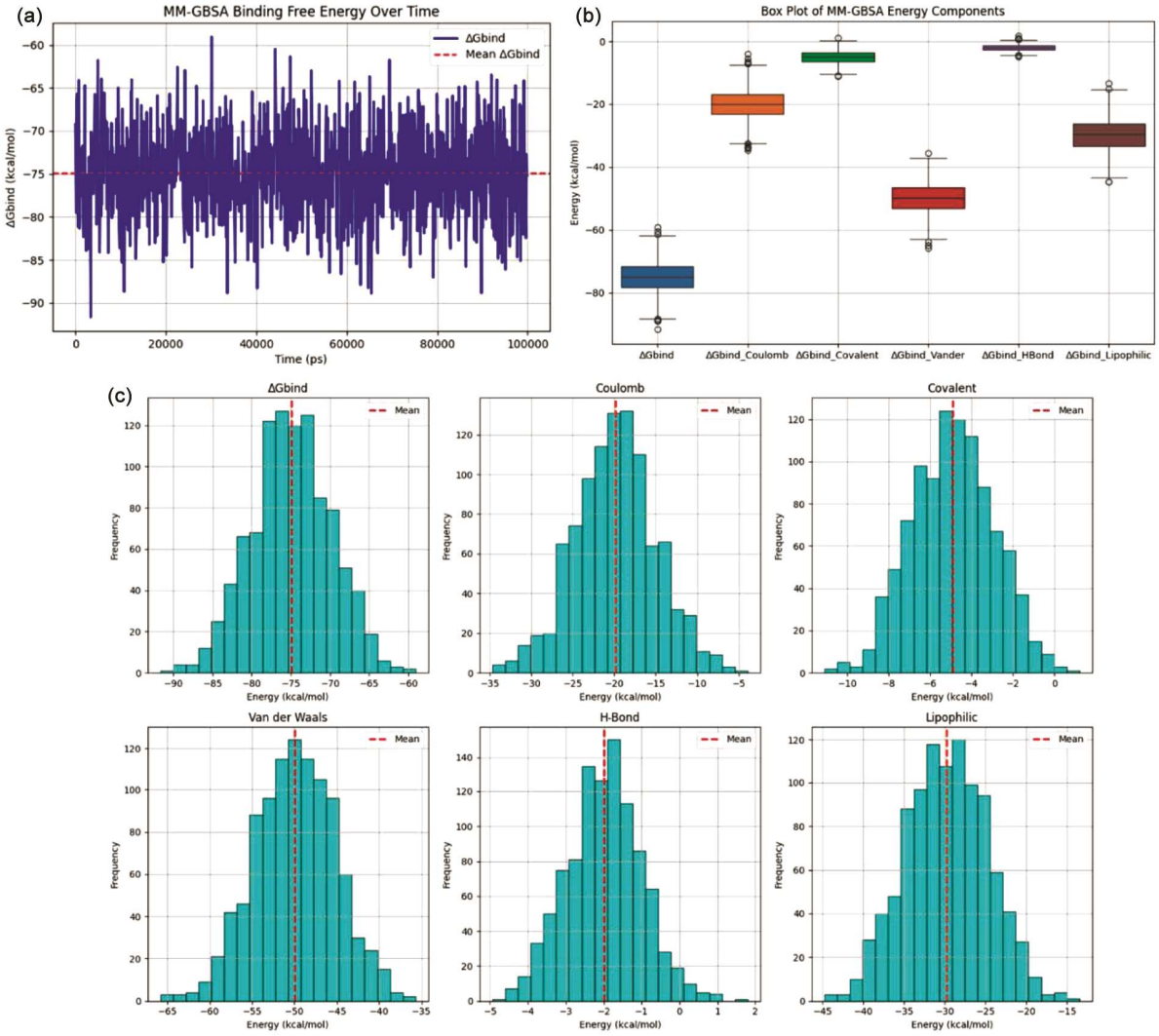

Fig. 15 — MM-GBSA ligand–protein complex binding free energy evaluation over 100 ns molecular dynamics simulation. (a) Stable binding energy is indicated by the temporal progression of ΔG_bind; (b) The box plot shows energy components such as Coulombic, van der Waals, covalent, hydrogen bond, and lipophilic interactions; and (c) Histograms show the frequency distribution of energy components, emphasizing the importance of van der Waals and electrostatic forces in complex stabilization

results. The ligand showed prolonged binding, mostly due to hydrophobic and electrostatic interactions, indicating it might cure Alzheimer's disease.

DFT calculation

According to Koopmans' theorem, global reactivity descriptors were calculated using DFT values for the HOMO and LUMO orbitals. Table 4 shows that one Hartree equals 27.2114 electron volts (eV). Quantum chemical descriptors showed intermediate stability and reactivity for the compound. The ionization potential was 6.089 eV and the electron affinity was 0.902 eV, suggesting considerable electron donation and acceptance. The electronegativity is 3.495 eV,

Table 4 — DFT-based global reactivity descriptors

Property	Value (eV)
Ionization Potential (I)	6.089
Electron Affinity (A)	0.902
Electronegativity (χ)	3.495
Chemical Hardness (η)	2.598
Chemical Potential (μ)	–3.495
Chemical Softness (S)	0.385 eV^{-1}
Electrophilicity (ω)	2.355
Energy Gap (ΔE)	5.191

with chemical hardness and softness values of 2.598 eV and 0.385 eV^{-1}, respectively, indicating balanced charge transfer resistance. The chemical

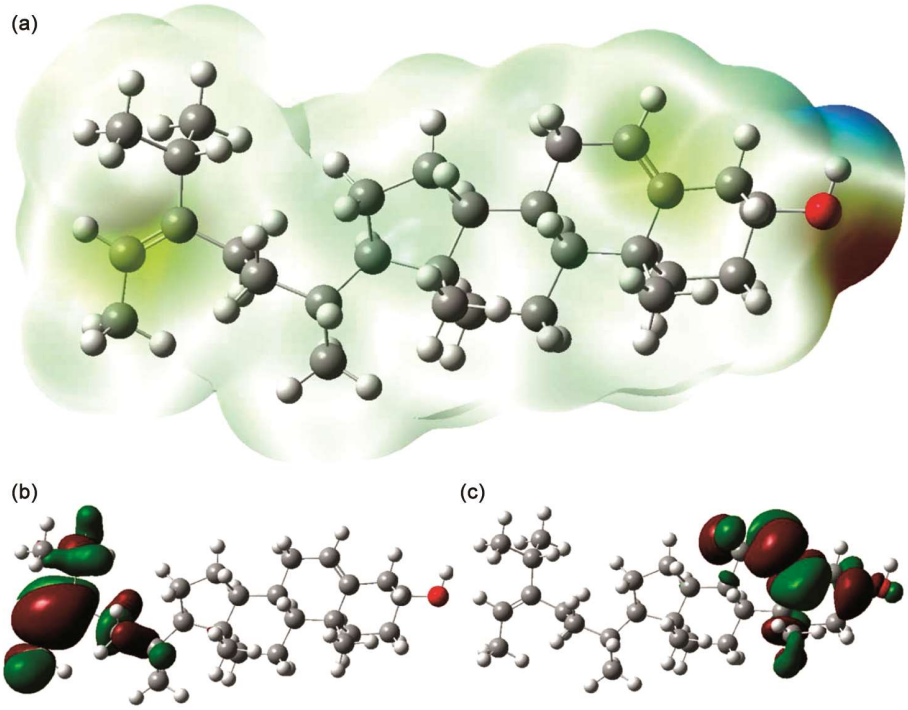

Fig. 16 — DFT analysis of fucosterol with (a) ESP; (b) HOMO, and (c) LUMO diagrams

potential was –3.495 eV, indicating full stability. An electrophilicity index of 2.355 eV and a stable electronic configuration with an energy gap of 5.191 eV showed that the molecule was moderately electrophilic.

The DFT study of fucosterol revealed its electrical structure and reactivity. Figure 16 a shows the electrostatic potential (ESP) surface, showing molecular charge distribution and electron density. The red zone surrounding the hydroxyl group has high electronegativity, indicating hydrogen bonding or nucleophilic interactions. Blue and green parts of the hydrocarbon backbone indicate chemical inertness due to neutral to slightly electron-rich zones.

The highest occupied molecular orbital (HOMO) is around the hydroxyl group and neighboring carbon atoms in (Fig. 16b). This localization shows that specific locations donate electrons during molecule interactions, perhaps impacting binding affinity. In Figure 16c, the LUMO was at the side chain at the molecule's distal end. The spatial difference between HOMO and LUMO orbitals suggests intramolecular charge transfer owing to chemical reactivity and contact with electron-rich protein residues.

Limitations

Despite being extensive, this research has several drawbacks. In-silico methods like molecular docking and molecular dynamics simulations are used, however they cannot completely replicate the complex biochemical environment of the human brain. Second, the work lacks *in vitro* or *in vivo* experimental confirmation of molecular interactions and neuroprotection. Thirdly, the phytochemical dataset was acquired from literature and databases, which may not include all *Cassia fistula* metabolites. MD simulations reduced membrane effects.

Conclusion

This research suggests *Cassia fistula* may contain neuroprotective chemicals that targ*et al*zheimer's disease-related inflammation. Among the phyto constituents tested, fucosterol had high binding affinity and dynamic stability with SRC kinase, a neuroinflammatory pathway regulator. Molecular docking, molecular dynamics simulations, MM/GBSA energy analysis, and DFT calculations show fucosterol's inhibitory potential, stable connections, and favorable electronic properties. *In vitro* and *in vivo* validation of *Cassia fistula*-derived compounds for plant-based neurological treatments is supported by computational findings.

Future Prospective

Future study should utilize *in vivo* models to assess active chemical pharmacokinetics, blood-brain barrier

penetration, and efficacy. It is recommended to perform functional validation of targets like STAT3 and SRC by gene editing methodologies. The incorporation of 3D neural cells or brain organoids with multi-omics methodologies may provide improved mechanistic understanding.

Acknowledgement

We thank all the affiliated colleges for providing resources and computational support to conduct this research. This work was supported by the Deanship of Scientific Research, Vice Presidency for Graduate Studies and Scientific Research, King Faisal University, Saudi Arabia [Grant No. KFU252840].

Conflict of interest

All authors declare no conflict of interests.

References

1 Gote S, Dubey S, Nargund SL & Thapa S, *In silico* investigation of coumarin-based compounds targeting Keap1-Nrf2 pathway involved in the development of Alzheimer's disease. *Lett Drug Des Discov*, 22 (2025) 69241.

2 WHO, Dementia [Internet]. WHO. 2024 [cited 2025 May 27]. Available from: https://www.who.int/news-room/fact-sheets/detail/dementia

3 Marucci G, Buccioni M, Ben DD, Lambertucci C, Volpini R & Amenta F, Efficacy of acetylcholinesterase inhibitors in Alzheimer's disease. *Neuropharmacology*, 190 (2021) 108352.

4 Dawkins E, Derks R JE, Schifferer M, Trambauer J, Winkler E & Simons M, Membrane lipid remodeling modulates γ-secretase processivity. *J Biol Chem*, 299 (2023) 103027.

5 Arafi P, Devkota S, Williams E, Maesako M, Wolfe MS, Alzheimer-mutant γ-secretase complexes stall amyloid β-peptide production. *Elife*, 13 (2025) 1.

6 Devkota S, Williams TD & Wolfe MS, Familial Alzheimer's disease mutations in amyloid protein precursor alter proteolysis by γ-secretase to increase amyloid β-peptides of ≥45 residues. *J Biol Chem*, 296 (2021) 100281.

7 Heneka MT, van der Flier WM, Jessen F, Hoozemanns J, Thal DR & Boche D, Neuroinflammation in Alzheimer disease. *Nat Rev Immunol*, 25 (2024) 321.

8 Kuznetsov IA & Kuznetsov AV, How the formation of amyloid plaques and neurofibrillary tangles may be related: A mathematical modelling study. *Proc R Soc A Math Phys Eng Sci*, 474 (2018) 1.

9 Amin E, Elgammal YM, Zahran MA & Abdelsalam MM, Alzheimer's disease: new insight in assessing of amyloid plaques morphologies using multifractal geometry based on Naive Bayes optimized by random forest algorithm. *Sci Rep*, 13 (2023) 1.

10 Valiukas Z, Tangalakis K, Apostolopoulos V & Feehan J, Microglial activation states and their implications for Alzheimer's disease. *J Prev Alzheimer's Dis*, 12 (2025) 100013.

11 Afridi R, Rahman HM & Suk K, Implications of glial metabolic dysregulation in the pathophysiology of neurodegenerative diseases. *Neurobiol Dis*, 174 (2022) 105874.

12 Wen X & Hu J & Targeting STAT3 signaling pathway in the treatment of Alzheimer's disease with compounds from natural products. *Int Immunopharmacol*, 141 (2024) 112936.

13 Yulion R, Andriani L & Aliyah SH, Network pharmacology and molecular docking identify the potential mechanism and therapeutic role of *Scutellaria baicalensis* in Alzheimer's disease. *Drug Des Devel Ther*, 18 (2024) 1497.

14 Zheng Y, Zhang X, Zhang R, Wang Z, Gan J & Gao Q, Inflammatory signaling pathways in the treatment of Alzheimer's disease with inhibitors, natural products and metabolites. *Int J Mol Med*, 52 (2023) 1.

15 Dhawan G & Combs CK, Inhibition of Src kinase activity attenuates amyloid-associated microgliosis in a murine model of Alzheimer's disease. *J Neuroinflammation*, 9 (2012) 1.

16 Sharma A, Kumar A & Jaitak V, Pharmacological and chemical potential of *Cassia fistula* L. – A critical review. *J Herb Med*, 26 (2021) 100407.

17 Garg R, Mohd I & Sharma V, Pharmacological and pharmacognostical studies of *Cassia fistula* Linn. *Indian J Health Care Med Pharm Pract*, 4 (2023) 107.

18 Saeed M, Naseer S, Hussain S & Iqbal M, Phytochemical composition and pharmacological effects of *Cassia fistula*. *Sci Inq Rev*, 4 (2020) 59.

19 Sliwoski G, Kothiwale S, Meiler J & Lowe E W, Computational methods in drug discovery. *Pharmacol Rev*, 66 (2014) 334.

20 Pandey B, Thapa S, Kaundinnyayana A & Panta S, Hepatoprotective effects of *Juglans regia* on carbon tetrachloride-induced hepatotoxicity: *In silico*/ *in vivo* approach. *Food Sci Nutr*, 12 (2024) 6482.

21 Pandey B, Thapa S, Biradar MS, Singh B, Ghale JB & Kharel P, LC-MS profiling and cytotoxic activity of *Angiopteris helferiana* against HepG2 cell line. *PLoS One*, 19 (2024) 1.

22 Heberle H, Meirelles V G, da Silva F R, Telles G P,& Minghim R, InteractiVenn: A web-based tool for the analysis of sets through Venn diagrams. *BMC Bioinformatics*, 16 (2015) 1.

23 Li XM, Li MT, Jiang N, Si YC, Zhu MM & Wu QY, Network pharmacology-based approach to investigate the molecular targets of sinomenine for treating breast cancer. *Cancer Manag Res*, 13 (2021) 1189.

24 Zhang X, Shen T, Zhou X, Tang X, Gao R & Xu L, Network pharmacology-based virtual screening of active constituents of *Prunella vulgaris* L. and the molecular mechanism against breast cancer. *Sci Rep*, 10 (2020) 1.

25 Sequeira JC, Rocha M, Alves MM & Salvador AF, UPIMAPI, reCOGnizer and KEGGCharter: Bioinformatics tools for functional annotation and visualization of omics datasets. *Comput Struct Biotechnol J*, 20 (2022) 1798.

26 Hennequin LF, Allen J, Breed J & Curwen J, Tetrahydro-2H-pyran-4-yloxy quinazolin-4-amine: A novel, highly selective inhibitor. *J Med Chem*, 49 (2006) 6465.

27 Bai L, Zhou H, Xu R, Zhao Y, Chinnaswamy K & McEachern D, A potent and selective small-molecule

degrader of STAT3 achieves complete tumor regression *in vivo*. *Cancer Cell*, 36 (2019) 498.
28 Mwangi RW, Macharia JM, Wagara IN & Bence RL, The medicinal properties of *Cassia fistula* L: A review. *Biomed Pharmacother*, 144 (2021) 112240.
29 Thapa S, Biradar MS, Banerjee J & Karati D, *In silico* approach for predicting the inhibitory effect of home remedies on SARS-CoV-2. *Makara J Sci*, 27 (2023) 194.
30 Gote S, Thapa S, Dubey S, Nargund S L & Biradar M S, Computational investigation of quinazoline derivatives as Keap1 inhibitors for Alzheimer's disease. *Informatics Med Unlocked*, 41 (2023) 1.
31 Colovos C & Yeates TO, Verification of protein structures: Patterns of nonbonded atomic interactions. *Protein Sci*, 2 (1993) 1511.
32 Eberhardt J, Santos-Martins D, Tillack AF & Forli S, AutoDock Vina 1.2.0: New docking methods, expanded force field, and Python bindings. *J Chem Inf Model*, 61 (2021) 3891.
33 Prasad S, Kurmi C, Thapa S & Karati D, Molecular docking and pharmacokinetic evaluations of curcumin-based scaffolds as MDM2–p53 inhibitors. *Discov Chem*, 2 (2025) 1.
34 Prasad S, Thapa S, Metri S M & Suresha M, Molecular docking and toxicity prediction of phytoconstituents of *Piper longum* against MAO-A. *Discov Chem*, 2 (2025) 1.
35 Papaleo E, Mereghetti P, Fantucci P, Grandori R & De Gioia L, Free-energy landscape and structural clustering in molecular dynamics: The myoglobin case. *J Mol Graph Model*, 27 (2009) 889.
36 Vetrivel P, Murugesan R, Bhosale PB, Ha SE, Kim HH & Heo JD, Network pharmacology of prunetin-5-O-glucoside against gastric cancer. *Cancers (Basel)*, 13 (2021) 1.
37 Nyambo K, Tapfuma K I, Adu-Amankwaah F, Julius L, Baatjies L & Niang I , Molecular docking and simulations of *Mycobacterium tuberculosis* targets and bacterial metabolites. *Sci Rep*, 14 (2024) 1.
38 Al-Hamoud G A, Alam P, Fantoukh OI, Hawwal MF & Akhtar A, HPLC-UV analysis of chrysophanol in *Senna occidentalis* using ultrasonic extraction. *Processes*, 11 (2023) 1.
39 Münger LH, Boulos S & Nyström L, UPLC-MS/MS identification of dietary steryl glucosides. *Front Chem*, 6 (2018) 1.
40 Skubic C, Vovk I, Rozman D & Križman M, Simplified LC-MS method for sterols analysis in biological samples. *Molecules*, 25 (2020) 1.
41 Fernand VE, Dinh DT, Washington SJ, Fakayode SO, Losso JN & van Ravenswaay RO, HPLC determination of active compounds in *Cassia alata* root extracts. *Talanta*, 74 (2008) 896.
42 Hwang E, Park SY, Sun ZW, Shin HS, Lee DG & Yi TH, Protective effects of fucosterol against UVB-induced skin damage. *Mar Biotechnol*, 16 (2014) 361.
43 Azeez RA, Abaas IS & Kadhim EJ, Isolation and characterization of β-sitosterol from *Elaeagnus angustifolia*. *Asian J Pharm Clin Res*, 11 (2018) 442.
44 Hua Y, Yuan X, Shen YH, Wang J, Azeem W & Yang S, Novel STAT3 inhibitors targeting SH2 dimerization domain. *Front Pharmacol*, 13 (2022) 1.
45 Kumar S, Kumar BH, Nayak R, Pandey S, Kumar N & Pai KSR, Computational screening of natural compounds against STAT3 SH2 domain. *Mol Divers*, (2025) 1.
46 Millot P, San C, Bennana E, Porte B, Vignal N & Hugon J, STAT3 inhibition protects against neuroinflammation and BACE1 upregulation. *Immunol Lett*, 228 (2020) 129.